CALT 68-502
ENERGY RESEARCH AND
DEVELOPMENT REPORT

PHOTON-COLLECTING HADRON CALORIMETERS*

F. J. Sciulli

California Institute of Technology, Pasadena, California 91125

Rapporteur talk on experimental information relating to photon collecting hadron calorimeters, presented at the FNAL Calorimetry Workshop, May 8-9, 1975.

*Work supported in part by the U.S. Energy Research and Development Administration. Prepared under Contract AT(11-1)-68 for the San Francisco Operations Office.

I. Introduction

Many years ago, while still a callow college youth, I heard rumors of some cosmic ray physicists[1] who had devised a technique for measuring the energies of cosmic rays (10^{11} to 10^{13} ev) by calorimetry. My mind immediately pictured the device shown in figure 1, which a little calculation showed would respond to such stimuli with a temperature rise of from 10^{-11} to 10^{-13}°K. Knowing the trouble that people had with measuring the temperature of the universe to even 3°K, I thought that these people must be exceedingly clever.

Their technique was not quite what I had pictured, in that they envisaged sampling with fast-pulse techniques the ionization energy in the resulting cascade. Even so, they were indeed clever, anticipating a method that has very wide application today at the high energy accelerators for the measurement of kinetic energy. It is not the first time that the techniques of high energy physics were pioneered by cosmic ray physicists.

In recent years, the use of these devices has been applied to measure total energy in hadron-induced reactions,[2] neutrino-induced reactions,[3] and will be used in the near future for muon-scattering experiments.[4] Although there are some recent attempts to use Cerenkov light[5] as the indicator of energy-loss, and some very sophisticated plans to use ionization chambers,[6] the most commonly used of these devices collect the photons from scintillation light given off by ionization in the hadronic cascade.

Conceptually, the simplest calorimeter is the total-absorption device in which all the ionization energy provides the observed photons. However, at high energies the sheer size and volume required for containment becomes prohibitive. For example, containment in pure liquid scintillator of a 100 GeV hadronic shower requires volume of order 2500 $ft.^3$. To solve the problem of containment and the corollary problems of size and cost, the more typical devices in use are sampling calorimeters, which allow a reduction in volume of order 10^3. These use a much heavier material, usually steel, as the principle medium for the cascade. Interspersed between steel plates are scintillation counters which sample the number of particles in the cascade at several locations. The sum of these samples gives, then, a measure of the total incident energy.[7]

The physics of hadron calorimeters is quite different from high energy electron or photon calorimeters. Although most of the ionization energy in the shower ultimately dissipates in electromagnetic cascades, from π°'s, the conversion of energy into π°'s occurs through strong interactions of charged hadrons (mostly $\pi^\pm$) with nuclei. Some of this energy is lost (e.g. nuclear binding energy) and some is typically sampled very badly (e.g. evaporation α's). This contrasts with purely electromagnetic showers, where very little energy is unobservable. The scale of distance is of course different from the electromagnetic case, and is more complicated. Whereas electron showers scale according to the radiation length, hadron showers depend on both radiation length (X_r) and interaction length (X_I). In heavy materials ($X_I \gg X_r$), containment should scale with X_I.

Figures 2 and 3 show, respectively, examples of a total absorption scintillation calorimeter[8] and an iron-plate sampling calorimeter[9] presently in use in experiments at FNAL. Of fundamental importance in the design of this kind of equipment are the balance among the various requirements. Although some experimenters may only desire hadron recognition, others may require extremely good energy resolution. In other cases, average resolution may be secondary to the absence of tails in the response curve. The requirements must be balanced against the availability of resources; i.e. size and shape, cost, etc.

In this talk, I will address myself primarily to the question of resolution in photon-collecting hadron calorimeters. The major properties for optimization of resolution will be discussed: (1) necessary size for containment and the effect of non-containment on resolution; (2) optimization of sampling frequency and (3) related questions of unsampled energy.

Like most people who have built these detectors, we at Caltech have our own friendly Monte Carlo computer program for the calculation of calorimeter response. This program is perhaps the most naive of those described at this meeting, in that it calculates only the high energy component of the hadronic cascade, making the assumption that <u>no</u> nuclear disintegration energy is observed. The detailed dynamical assumptions are very close to the program outlined by Jones[10] a few years ago, with some additions related to transverse shower growth. This calculation was originally devised to explain and predict calorimeter response for thick samples (~ 10 cm), where it proves to be quite good. When referred to, in particular for questions of containment, it will be referred to as the calculation of the high energy shower component (HESC calculation).

My approach will be empirical whenever possible; i.e. to use the data itself to discuss relevant features of calorimeters. In the case of transverse containment, data is sorely lacking at the present time (though we are likely to have such information soon[11]); in this case, we will rely on the containment calculation to interpret the available data.

II. Containment

This topic divides itself naturally into two parts: longitudinal and transverse containment; i.e., the effect of energy escaping the back and sides, respectively, of the calorimeter. The longitudinal containment will surely be directly related to the total mass of the device along the beam direction. I will use as an indicator of longitudinal containment, D_s = total length of steel along the beam. For transverse containment, the effect of gaps (e.g. containing scintillator sampling stations) must be taken into account. As an indicator of transverse containment, I will use R_s = radius of an equivalent solid steel target. That is, for a calorimeter of actual steel radius, R, and packing fraction, $p = {}^{\text{steel}}/(\text{steel} + \text{gaps})$, then this "scaling rule" would suggest that an equivalent solid target would have radius $R_s = pR$.

Table I shows a summary of the photon collecting hadron calorimeters reporting results up to the present time. The containment indicators, D_s and R_s, are shown along with the actual dimensions of the devices. I will now turn to measurements relating these indicators to actual containment and the resulting effects on resolution.

The earliest published experimental work on longitudinal containment came from a CERN group,[12] who compared the pulse height distributions at several depths inside a steel target with their Monte Carlo calculations and found good agreement (see fig. 4). The actual criteria for containment are not, unfortunately, directly experimental in this case, but come from the same Monte Carlo calculation. The relative calculated resolution as a function of steel depth, D_s, and radius, R_s, of a solid steel target is shown in figure 5 over the energy range $3 \leq E \leq 20$ GeV. They conclude that $D_s > 1$ meter and $R_s > 30$ cm in solid steel are required for good containment.

The Harvard-Penn-Wisconsin-Fermilab (HPWF) group[8] has built and used the only pure liquid scintillator in calorimeter in Table I. This device, built as a neutrino detector, is of relatively enormous dimensions (see fig. 2). Its size is such that it will contain hadronic cascades initiated near the front end, up to about 100 GeV in total energy. This provides a unique opportunity to study a sampling calorimeter that is all "sample". Figure 6 shows their experimental data on relative energy observed as a function of depth. They have parametrized these curves in terms of a median penetration depth, z_p, which is the depth at which half of the total observed energy has been deposited. A good fit to the data is

$$z_p = 45.7 \log_e \frac{E(\text{GeV})}{0.38} \qquad \text{in cm of scintillator}$$

Figure 7 shows an almost universal curve for the relative integrated containment vs. $z_R = {}^{z}/z_p$. In figure 8, the required depth in <u>scintillator</u>, D_{sc}, is shown for fixed fractional energy containments of 70% and 90%. I have calculated these curves directly from their parametrical data fits.

The Caltech-Fermilab (CITF) test calorimeter,[13,14] a half percent scale model of the neutrino calorimeter, is shown in figure 9. With 10 cm steel spacing, it is the thickest sampling calorimeter of the entire group. The counters were individually pulse-height analyzed and recorded on magnetic tape so that cuts could be later applied to examine containment and spacing effects. In figure 10, the response of the calorimeter vs. depth is compared to the HESC calculation for two very different incident energies. Figure 11 shows the overall response and resolution of the device as a function of incident energy. The effect of calorimeter length, D_s, on relative response and relative resolution at 200 GeV are shown in figure 12. Very little improvement in either response or resolution are gained for lengths greater than about 1 meter of steel. The curves, from the HESC calculations, reproduce the data quite reasonably.

The solid lines in Figure 13 are the results of the HESC calculation for required steel length, D_s, for fixed fractional energy containment, f. Also shown are the calculated effect on resolution. The lengths for fixed containment as observed in the CITF apparatus, shown as data points, are in reasonable agreement over the range $5 < E < 200$ GeV and provides an experimental check on the calculations.

Two very interesting points should be made with regard to this figure. First, the effect on resolution can be quite large for even a small loss of energy out the back of the device. For example, a 5% loss of energy can broaden the resolution by $\geqslant$ 25% of the resolution with perfect containment.

A second important feature is obtained by superimposing the experimental containment curves (from figure 8) of the liquid scintillator HPWF calorimeter, shown as dashed lines. These have been scaled by the ratio of scintillator density to steel density. The CITF points, in essentially pure steel, are contained within the HPWF limits measured in scintillator. We can, therefore, conclude the following: (1) The length of calorimeter required for fixed fractional containment scales with density between mineral oil (scintillator) and steel. (2) The required length varies in both cases approximately as $\log_e \frac{E(\mathrm{GeV})}{0.38}$.

In figure 14, the calculated longitudinal containment curves are shown again with the values of D_s displayed appropriate to the various calorimetry measurements. Typically, the containments are greater than 95%. In a few cases, it is not so; in particular, one of the configurations of BPW at low energy, the higher energy data of HPWF ($E > 100$ GeV), and the CMS data. This latter experiment was triggered quite differently from the others, and we will consider it separately.

The calculated transverse containment curves are shown in figure 13, with the values of R_s appropriate to the experimental data. It should be noted that there is very little experimental data to check these calculations. In the following discussions, I will concentrate on data which contained more than 95% of the shower. With the exception of the FCIT test,[16] which used small scintillator counters; the experiments typically contained more than 95% of the shower energy.

One rather important point remains to be made before leaving the question of containment. Although the RMS width of response curves is rather seriously compromised by lack of containment, the effect can be more drastic than measured by this single parameter. Figure 16 shows response curves from the CITF[14] data at 150 GeV. The narrow curve is the total response for the full length (142.8 cm steel) calorimeter, for which more than 99% of the energy is contained. The broader distribution is for the same data summed over only half of the full length, which contains roughly 90% of the energy. The general broadening of the distribution described above is readily apparent. Even more important in many applications, however, is the development of the low energy tail in the uncontained curve, which is not observed in data with full containment.

In order to make sensible comparisons, I will primarily concentrate the following discussions on data which contained $\geqslant$ 95% of the shower energy.

III. Sampling Frequency

The resolution of sampling calorimeters might reasonably be expected to be dependent upon the thickness, s, of steel between samples. This discussion will separate two regimes of sampling for which data exists: (1) thick sampling, $s \geq 10$ cm. steel; and (2) thin sampling, $0 \leq s \leq 10$ cm. steel.

(1) Thick sampling ($s \geq 10$ cm. steel).

The principle limitation for the cruder sampling frequency is expected to be the fluctuations at specific locations of the electromagnetic showers from the $\pi^{\circ} \rightarrow \gamma + \gamma$ decays. These produce the largest single fraction of ionization energy in the entire hadronic cascade. Figure 17 shows the electromagnetic cascade in number of electrons vs. depth in steel as calculated from Rossi's formula.[19] Over much of the range in energies displayed, three samples of the shower can be obtained with 10 cm sampling. Much cruder spacing, however, would result in two samples or less. The result in such circumstances would depend on where precisely the cascade initiated. This qualitative feature is borne out by the data. Figure 18b shows the RMS resolution for the 200 GeV data vs. sampling thickness, s, in inches. Between $10 < s < 30$ cm, the resolution broadens almost linearly, and beyond 30 cm becomes worse than linear. The effect between 10 and 20 cm is almost energy-independent, as shown in figure 18a. The 10 cm resolutions, shown in figure 11, uniformly become worse by a factor of 2 over the entire energy range when the sample thickness, s, is doubled. This is in sharp contrast to the electromagnetic-shower case where the resolution worsens like the square-root of thickness over a wide range.[20]

(2) Thin sampling ($0 \leq s \leq 10$ cm. steel).

There appears in the presently available data, two different regimes in energy where the effect on resolution is qualitatively different. Figure 19 shows the RMS resolution for $E \geq 100$ GeV. The three data groups were taken with pure scintillator, 3.8 cm. steel spacing, and with 10 cm spacing, respectively. Although there may be some small resolution differences, no systematic pattern with sample frequency is evident. Within about 20%, the resolution appears to be independent of sample thickness, s. This contrasts sharply with the thick sampling case discussed above.

The lower energy, thin-sampling case is presented in figure 20 for the data with good containment. At the lower energies, there is clear difference between the 10 cm sampled data and the data with $s \leq 2.5$ cm. By 100 GeV, the differences disappear, but at 20 GeV, there is over a factor of 2 difference in resolution. In addition, for $E > 10$ GeV, there is no discernable differences[21] in the performance of devices with $s = 2.5$ cm steel, and with $s = 0$ cm. Superimposed on this data is the calculated curve from the HESC calculations for the ideal resolution of a device that sees no nuclear disintegration energy, but samples perfectly all the ionization in the high energy shower. Quite clearly, with 2.5 cm spacing, some nuclear disintegration energy is being observed and is improving resolution. This is, I feel, an important point to which we shall return later.

In figure 21, some additional data is shown, much of which was taken with less than adequate containment. One very important anomoly is apparent in the CMS data[17] which bears some discussion. That data taken with $s = 2$ cm, falls below the data in pure scintillator, $s = 0$ cm. The anomoly can be explained, I believe, by the unique triggering configuration of the CMS experiment. Their calorimeter was too small to longitudinally contain typical showers at their higher energies. They chose to trigger their data-taking by vetoing any event that had energy escaping the downstream end of the calorimeter. The curve labelled "Anti" in figure 22 shows the fraction of all events removed by this condition. For example, the 5% resolution at 60 GeV is obtained on only 30% of all protons interacting in their calorimeter. The selection, of course, preferentially picks events that deposit all their energy upstream in the calorimeter. Since π° showers are absorbed more quickly than hadronic showers, the.

recorded events are very likely to be those that turn a large fraction of their energy into π°'s at an early stage and are, therefore, less sensitive to fluctuations in unobserved nuclear disintegration energy. At any rate, and with any physics explanation, the very fact that they were able to improve their resolution substantially by a simple cut in the data depending only on a crude longitudinal deposition requirement, means that important information resides in the longitudinal energy distribution for individual events. One very important problem which should be addressed is to find the most appropriate algorithim to incorporate this information in the most efficient manner.

IV. Unsampled Energy

In the process of equalizing the gains of phototubes in calorimeters, muons are often transmitted and their pulse heights recorded. If the energy loss of the muons in steel is known (from calculation), the calorimeter will have an absolute calibration, i.e. energy loss/unit pulse height. The net response to hadrons of some known beam energy then allows a measure of the fraction of energy, F, sampled by the device. This procedure is prone to a number of systematic differences between experiments. An alternative procedure, to compare hadrons of fixed energy with electrons of the same energy is sensitive to different problems, including transition effects for different materials.[22] One might expect either of these methods to measure the sampled energy fraction, to ~5-10%. Within this error, experiments to date, for energies above 50 GeV, consistently give $70 < F < 80\%$, essentially independent of sampling fraction. (See figure 23). It is clear that roughly 25% of the energy is unsampled in such devices, but real differences in relation to sampling frequency, or more likely, fraction of the calorimeter that is active, must await more precise experiments.

At lower energies, $E < 20$ GeV, a smaller fraction of the energy is sampled. We would expect observable differences between pions and protons at fixed beam momentum at lower energies. Figure 24 shows the response curves in the BPW data[15] for 15 GeV/c protons and pions. Much of this difference in the peak can be attributed to the unsampled proton mass energy. Figure 25 shows the data on the ratio of the mean pion response to the mean proton response vs. momentum. The smooth curve, which is the ratio of kinetic energies at fixed momentum, follows the trend of the data but lies 2-5% below the data. Therefore, at fixed kinetic energy, the pion response is only 2-5% higher than proton response.

The data support the conclusion that nuclear disintegration energy losses are important for resolutions. In the light of the experimental results, especially for small samples (see section II), it might be of some interest to see if the qualitative behavior of high energy collisions with nuclei provide a clue to why such effects should be most visible for samplings less than about 2-3 cm.

The nuclear interactions that can be of importance are those that either (1) occur in the scintillator itself, or (2) occur in the steel but have some energy escaping into the scintillator. According to Murzin[23], the total number of nuclear interactions that occur in the entire shower are roughly as shown in table II.

Table II: N_o = typical number of nuclear interactions in shower

E_o	N_o	Number in scintillator for fractional mass of 3%
40 Gev	25	0.75
300 GeV	100	3.

For a fractional mass typical of the devices shown in table I, say 3%, the number of nuclear interactions is much too small to be of significance in the resolution.

The difference in resolution between 10 cm and 2 cm samples, must therefore be due to interactions occurring in the steel, but with secondaries energetic enough to be seen by the scintillator. Table III gives the different kinds of energy tabulated from emulsion cosmic-ray experiments.[23,24]

Table III: Nuclear Disintegration Energy

Energy Type	Fraction	Sampled
Evaporation Neutrons ($T \sim 8$ MeV)	.038	No
Evaporation Protons + α's ($T \sim 8$ MeV)	.062	No
Binding Energy	.114	No
"Fast" Neutrons ($T \sim 165$ MeV)	.393	secondary interactions $\left\{\begin{matrix}\text{binding } .17 \\ \text{evaporation } .22\end{matrix}\right\}$-No
"Fast" Protons ($T \sim 165$ MeV)	.393	Some
Total	1.000	

This component of fast protons, called "grey tracks" by cosmic ray physicists, has recently been directly observed in a calorimeter.[25] Interesting enough, the range for a 165 MeV proton is about 3 cm of steel. This component of the disintegration product should be sampled and providing resolution improvement, then, when $s \leqslant 3$ cm.

V. Questions

I would like to close by pointing out some of the gaps remaining in our experimental knowledge of calorimetry.

(1) Measurements of transverse containment and its effect on resolution are sorely needed over the entire energy range. An experimental check of the proposed "scaling rule" (see section II) would be very useful; if the effect of gaps in the device do not cause excessive leakage, the rule would make extrapolation to differing effective densities simple.

(2) Careful investigation of sampling on resolution is especially needed at low energy. Such work requires at least 99% containment and should investigate the following:

- (a) the effect of sampling size, s, with fixed fractional mass, F, in scintillator;
- (b) the effect of fractional mass with fixed sampling size, s.
- (c) the effect of different absorber material.

Though I must absorb the blame for the conclusions stated in this article, I should acknowledge that the work on calorimetry by the entire Caltech-FNAL group over the past few years has contributed in no small measure to the picture that has emerged here. I especially would like to thank Dr. A. Bodek with whom I have worked closely on our most recent data, and to Mr. D. Frank, who helped with the computer calculations.

References

1. N. L. Grigorov, V. S. Murzin, and I. D. Rapaport, J. Exptl. and Theoretical Phys. 34, 506 (1958) [Sov. Physics JETP 7, 348 (1958)].

2. For example E-111, E-379, FNAL.

3. For example E-21, E-1A, FNAL.

4. Private communications, L. Hand, W. Chen, S. Loken.

5. Private communication, B. Brown.

6. W. J. Willis, et.al., BNL Report 18813.

7. Up until the present there have been few attempts to use algorithms incorporating the longitudinal or transverse distribution in energy to improve resolution.

8. A. Benvenuti, D. Cline, W. T. Ford, R. Imlay, T. Y. Ling, A. K. Mann, F. Messing, J. Pilcher, D. D. Reeder, C. Rubbia, R. Stefanski, and L. Sulak (uncatalogued preprint).

9. L. W. Jones, J. P. Chanowski, M. J. Longo, P. L. Sleubic, J. L. Stone, and Bruce Cork, UM HE 73-24.

10. W. V. Jones, Phys. Rev. 187, 1868 (1969).

11. Private communication, M. Awschalom.

12. J. Engler, W. Flauger, B. Gibbard, F. Mönnig, K. Runge, and H. Schopper, NIM 106, 189 (1973).

13. B. C. Barish, J. F. Bartlett, D. Buchholz, T. Humphrey, F. S. Merritt, Y. Nagashima, F. J. Sciulli, D. Shields, H. Suter, G. Krafczyk, and A. Maschke, NIM 116, 413 (1973).

14. B. C. Barish, J. F. Bartlett, A. Bodek, K. W. Brown, D. Buchholz, F. Jacquet, F. S. Merritt, L. Stutte, F. J. Sciulli, H. Suter, H. E. Fisk, and G. Krafczyk, CALT 68-494.

15. F. Turkot, E. Harvey, T. Kondo, W. Kononenko, E. M. O'Neill, W. Selove, R. Diamond, A. R. Erwin, R. Loveless, M. Thompson, U. of P. Internal Report (uncatalogued).

16. S. Mori, J. Pine, and J. Scheid, TM-479 (FNAL).

17. Böhmer, et.al., NIM 22, 313 (1974).

18. W. V. Jones, et.al., NIM 72, 173 (1969).

19. B. Rossi, High Energy Particles (Prentice Hall, N.J., 1952), p. 214.

References - continued

20. I am indebted to David Yount for this observation.

21. W. Ford has pointed out that calculations by the Oak Ridge Group indicate that the pure scintillator device will be substantially better for $E < 10$ GeV. This is borne out by indirect measurements of resolution in the HPWF calorimeter using "quasi-elastic" events.

22. Private communication, W. V. Jones (LSU).

23. V. S. Murzin, Progress in Elementary Particle and Cosmic Ray Physics, Vol. 9 (North Holland, Amsterdam, 1967), p. 245.

24. C. F. Powell, P. H. Fowler, and D. H. Perkins, The Study of Elementary Particles by the Photographic Method (Pergamon Press, London, 1959).

25. Private communication, Prof. Yodh.

EXPTL. GROUP (ref)	S, Steel Sampling	Dimensions	Fractional Mass in Scintillator	D_s, Total Steel Length	R_s, Equivalent Solid Steel Radius	Energy Range
BPW (15)	1.27 cm 2.54 cm	120 x 120 x 250 cm^3	0.25 .14	57.2 cm 76.2	17 cm 27 cm	3-15 GeV
FCIT (16)	5.08 cm 10.16 15.24 20.32	Steel 30.5 x 30.5 x 183 cm^3 Scint. 18.4 x 33.0 cm^2	0.016 .008 .0054 .004	121.9 cm	8.9 cm (Scint!)	7,10,14 GeV
HPWF (8)	0	449 x 287 x 943 cm^3	1.00	943 cm sc. ≈103 cm Fe	203 cm sc. ≈22.1 cm Fe	14-144 GeV
CERN (12)	2.0	40 x 40 x 140 cm^3	0.04	80 cm	12.9 cm	6-24 GeV
CMS (17)	"	"	"	"	"	20-60 GeV
NASA (18)	2.7 cm	50 cm dia. x 95 cm	0.19	75.6 cm	20 cm	9-18 GeV
MA (9)	3.8 cm	61 x 61 x152 cm^3	0.02	114.3 cm	25.9 cm	200-300 GeV
CITF (13-14)	10.2 cm 20.4 cm	25.4 x 35.6 x181 cm^3	0.005	142 cm	13.3 cm	5-250 GeV

TABLE I.

EXPERIMENTAL WORK REPORTED

ON PHOTON COLLECTING HADRON CALORIMETRY

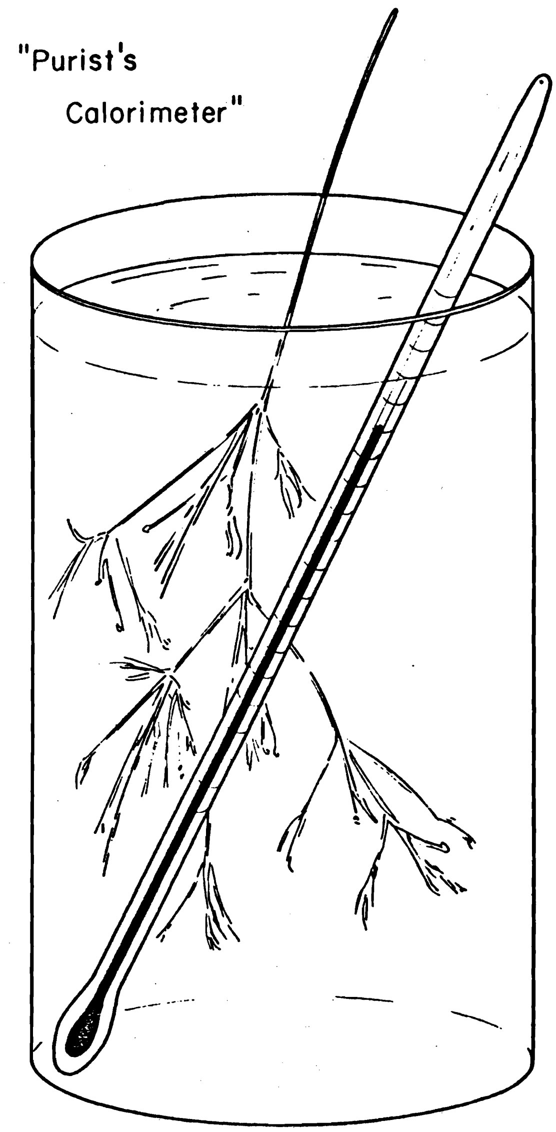

FIG. 1

FIG. 2

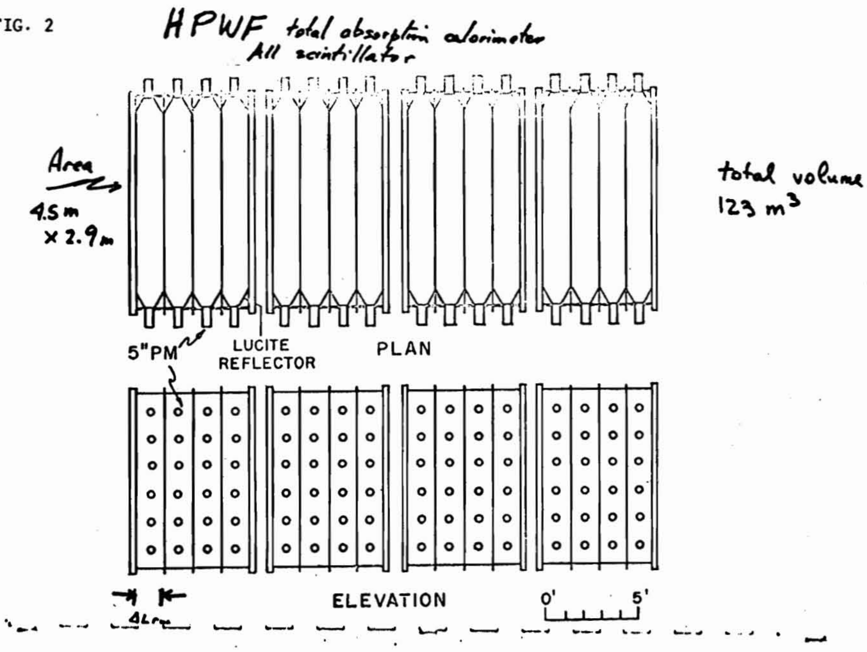

FIG. 3

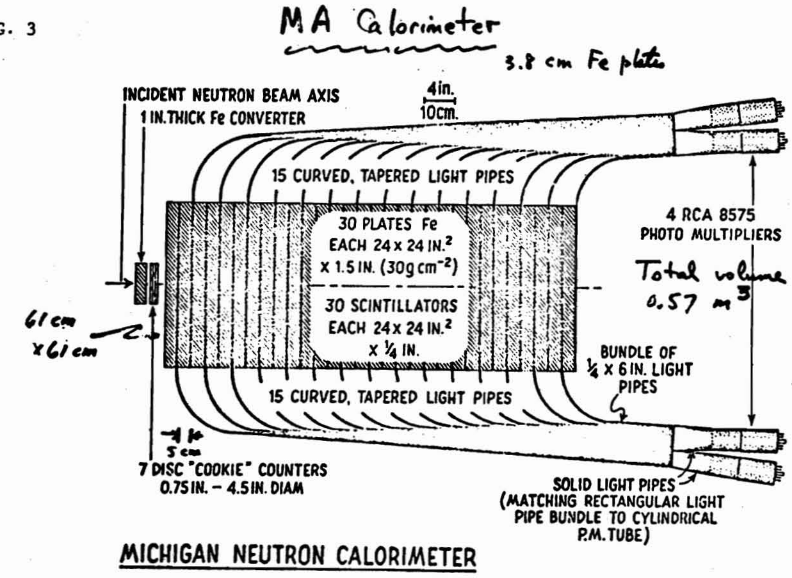

Plan view of the calorimeter.

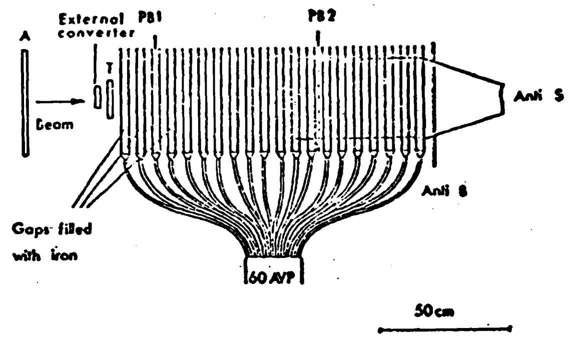

(a). Schematic layout of counter II with 40 scintillators. T is an external trigger counter; PB1 and PB2 are internal trigger counters. The counter A is in anticoincidence for neutrons and in coincidence for protons.

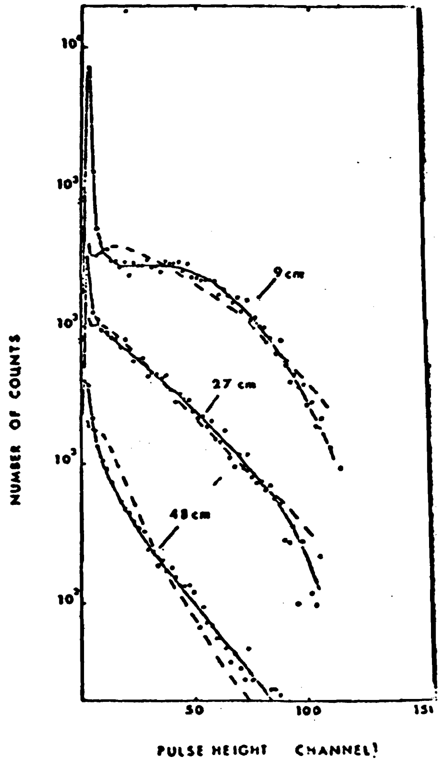

(b). Pulse-height distribution of the single probe counter ($40 \times 40 \times 1.5$ cm^3) behind different thicknesses of iron in the sandwich. The dashed curves were obtained from Monte Carlo calculations.

FIG. 4: CERN Calorimeter

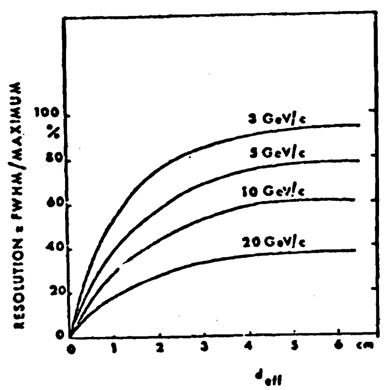

(c). The calculated resolution as a function of the effective thickness d_{eff} of the individual iron plates for different neutron momenta. The absorber size is very large.

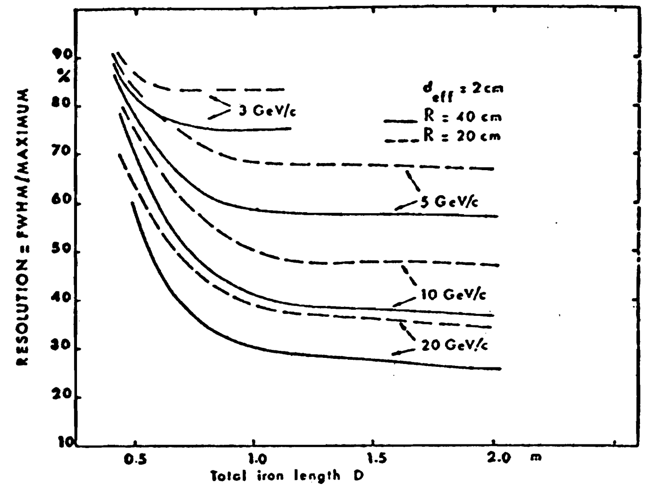

(a) • The calculated resolution as a function of the total iron length D for various momenta of incident neutrons. The curv refer to a radius of $R = 40$ cm and the dashed curves to $R = 20$ cm. The thickness of the individual iron plates is $d_{eff} = 2$ cm.

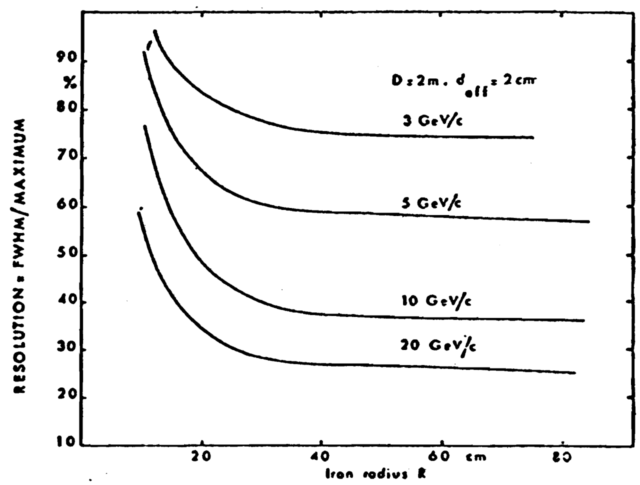

(b). The calculated resolution for a cylindrical STAC as a function of the radius R for different neutron momenta. The to iron thickness is $D = 1$ m and $d_{eff} = 2$ cm.

FIG. 5: Monte Carlo-calculated Resolutions vs. D_s (a), R_s (b) by CERN Group.

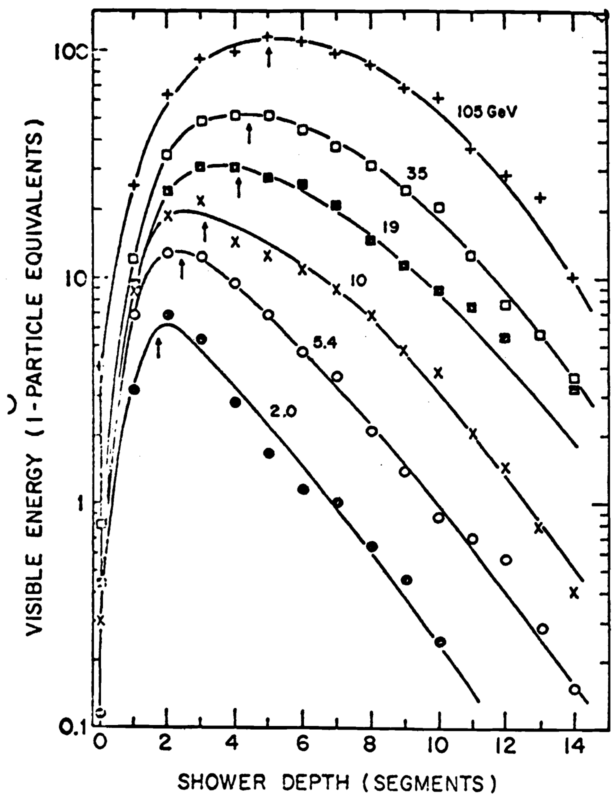

FIG. 6: RPWF data on longitudinal shower development in pure liquid scintillator (1 segment = 45.7 cm)

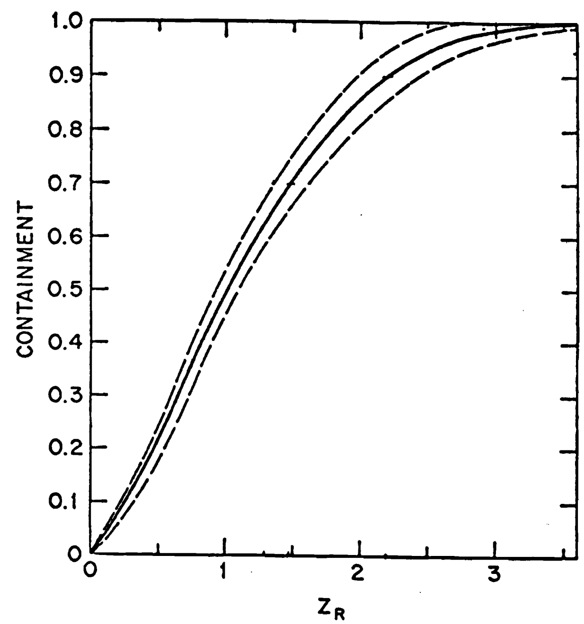

FIG. 7: Universal curve for containment in liquid scintillator vs. $Z_R = Z/Z_P$, where $Z_P = 45.7 \log \frac{E(\text{GeV})}{0.38}$ in cm.

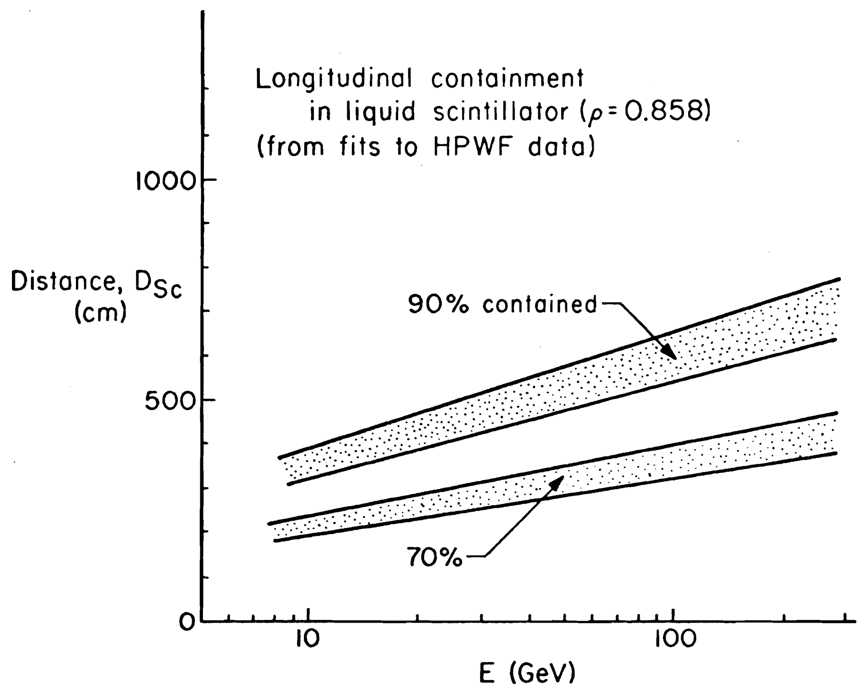

FIG. 8: Required longitudinal distance in liquid scintillator vs. energy.

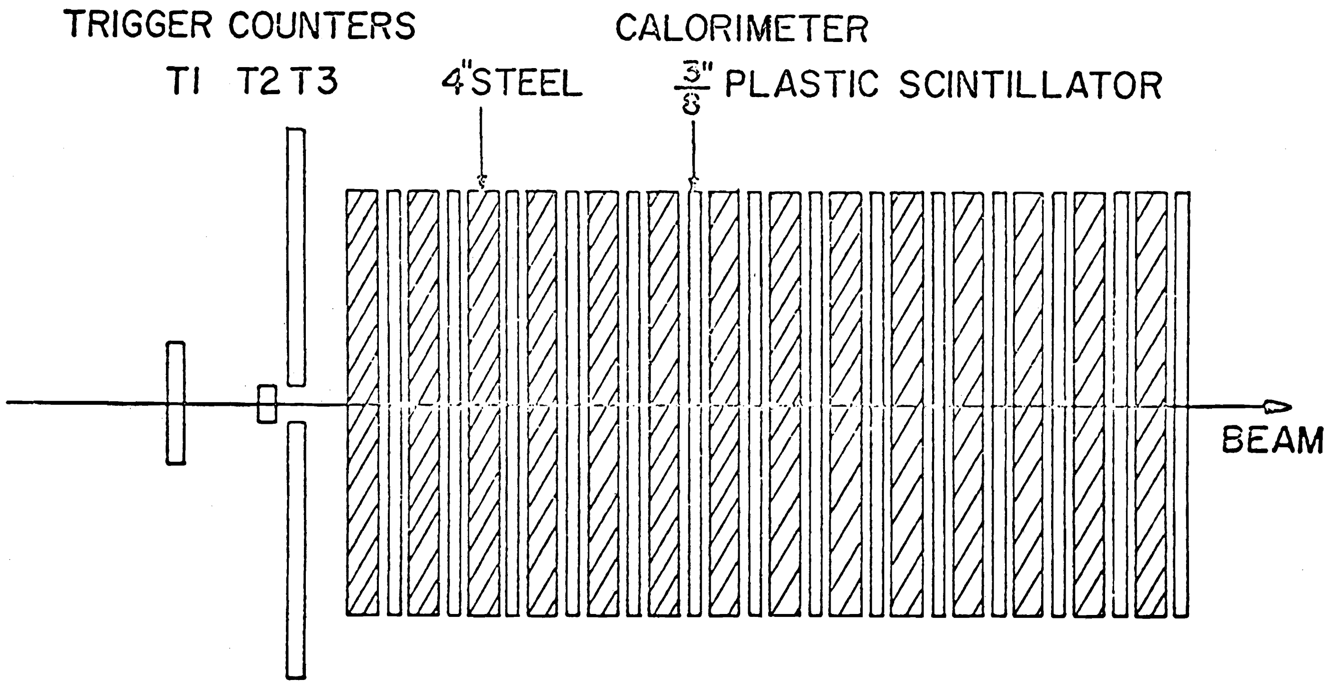

FIG. 9: Caltech-Fermilab test calorimeter, consists of half-percent of the actual neutrino calorimeter.

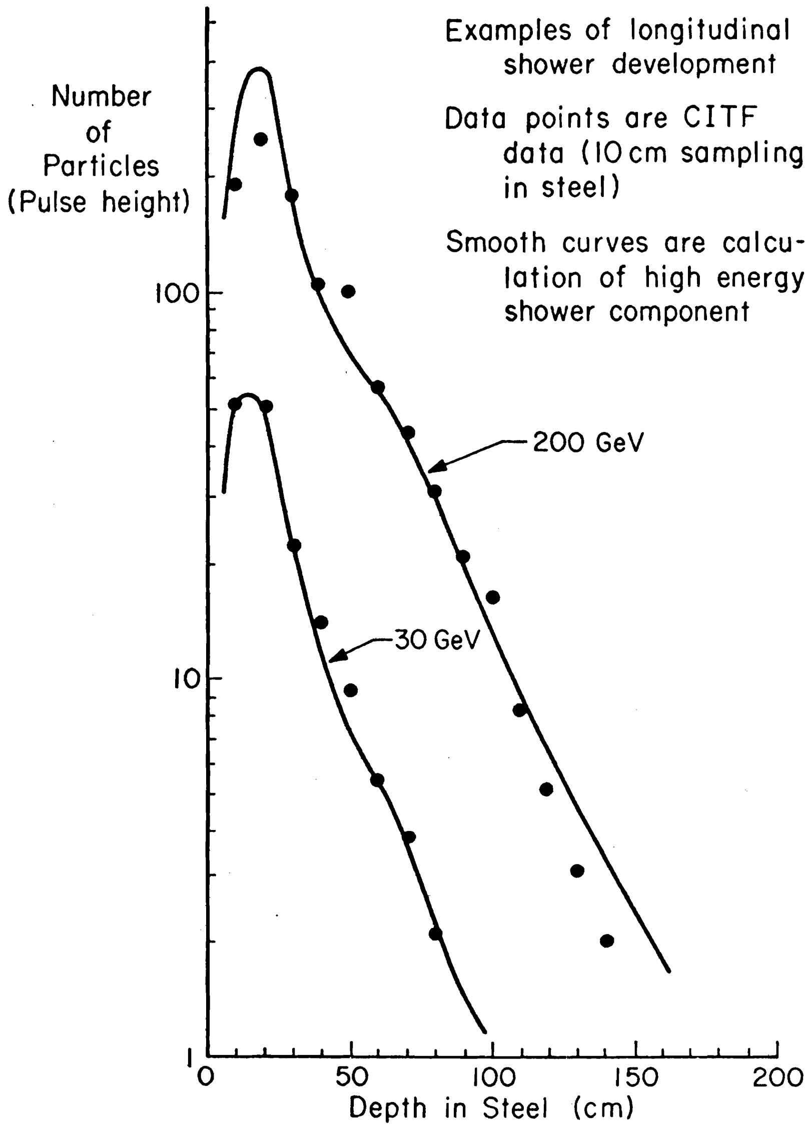

FIG. 10: CITF calorimeter response vs. depth in steel.

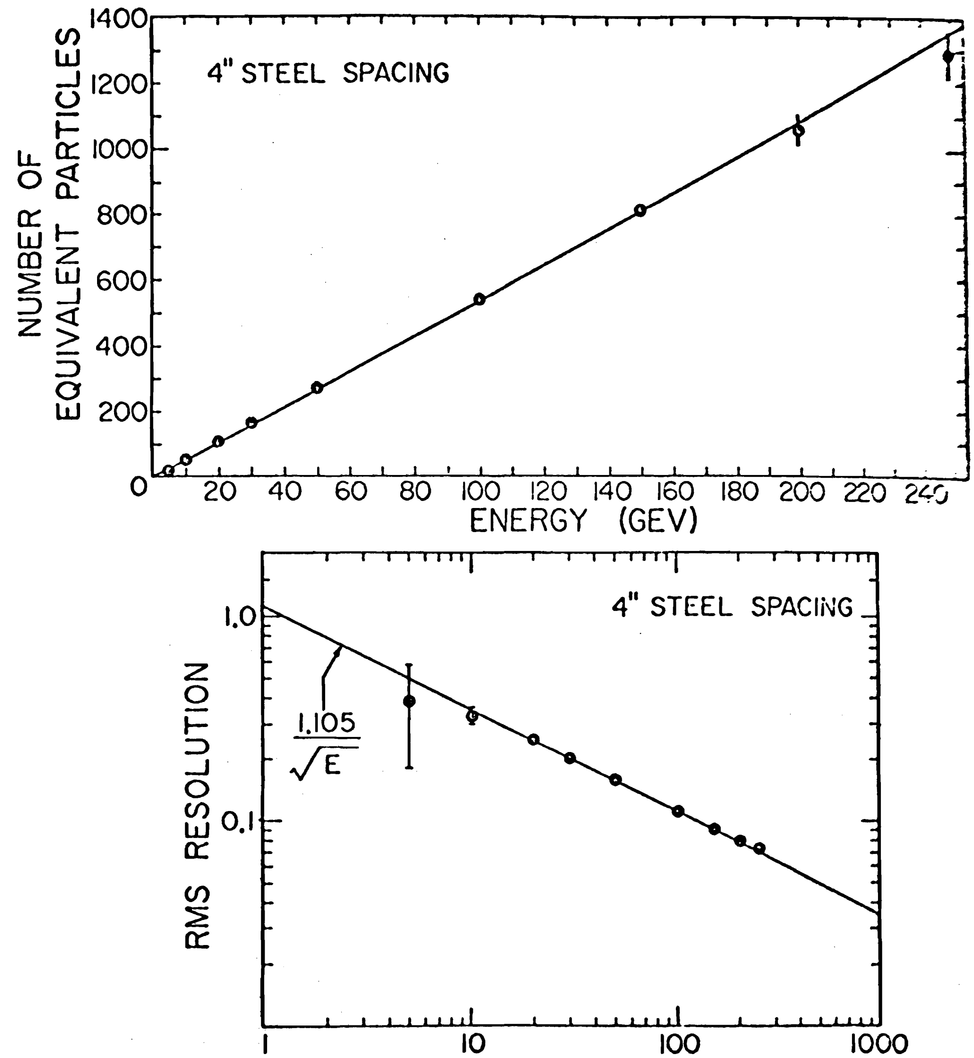

FIG. 11: Response and resolution of CITF calorimeter.

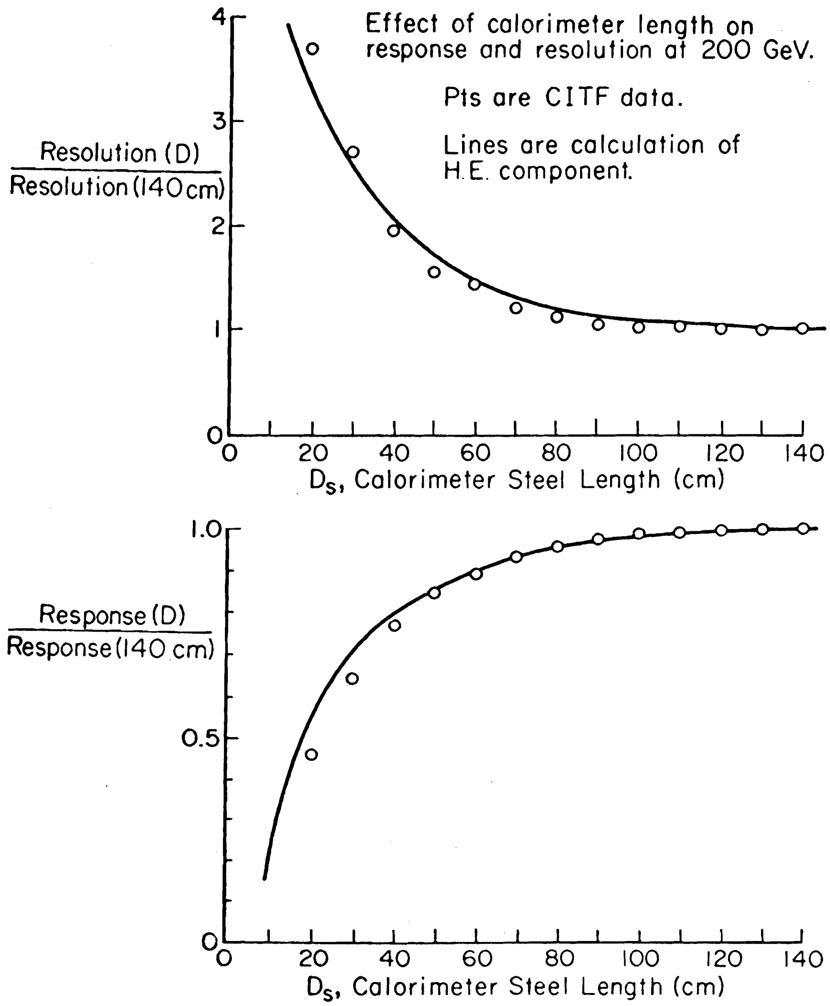

FIG. 12: Effect on resolution and response of longitudinal steel length.

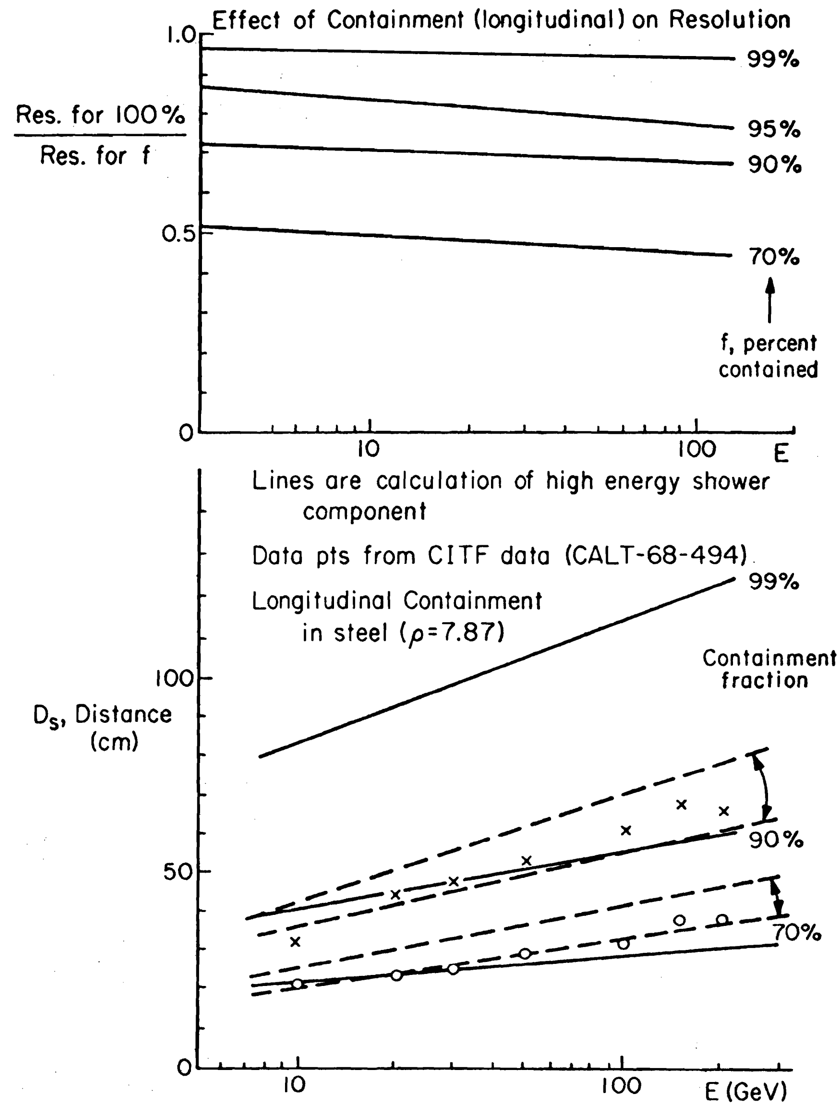

FIG. 13: Distance in steel (D_s) for given longitudinal containment. The pts. are the CITF data for 90% (x) and 70% (o) containment. The smooth curves are the results of the HESC calculation. The dashed lines are the HPWF data, taken in liquid scintillator (fig. 8), renormalized by the density ratio from scintillator to steel.

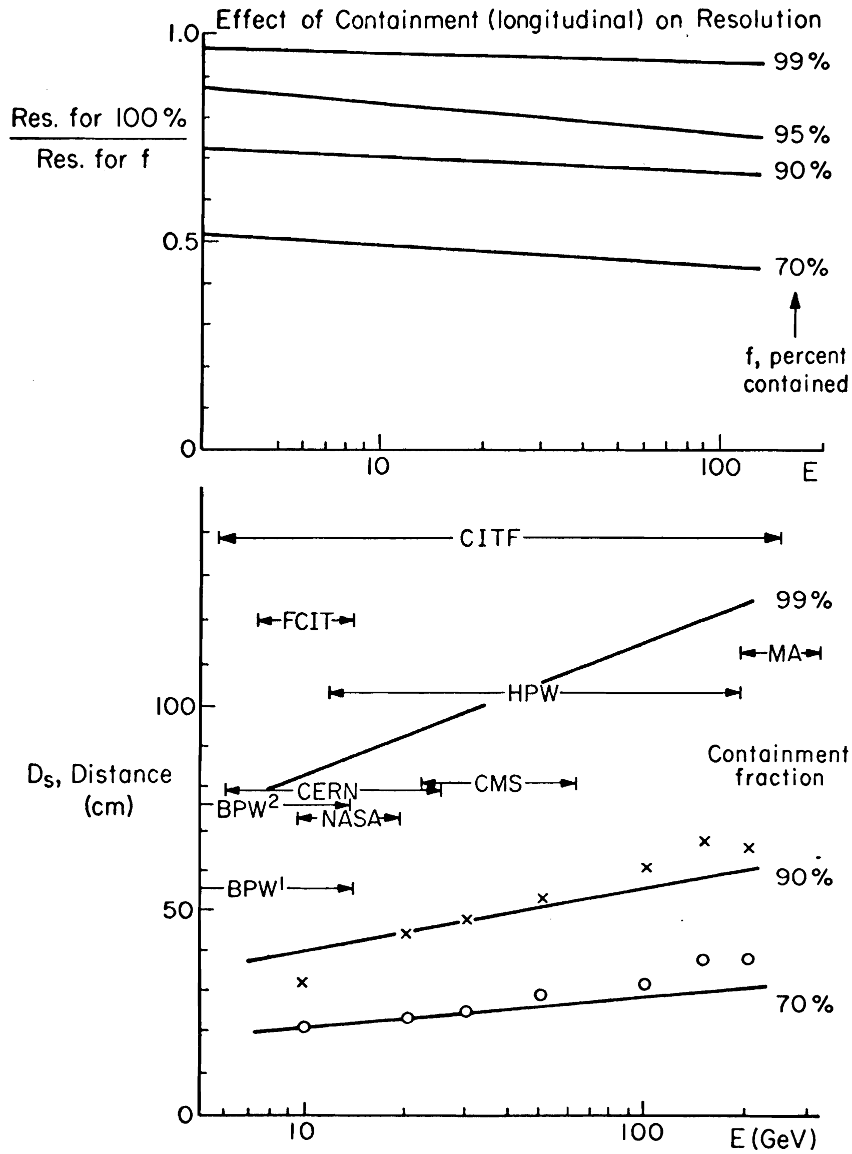

FIG. 14: Relative longitudinal containment for various calorimetry tests.

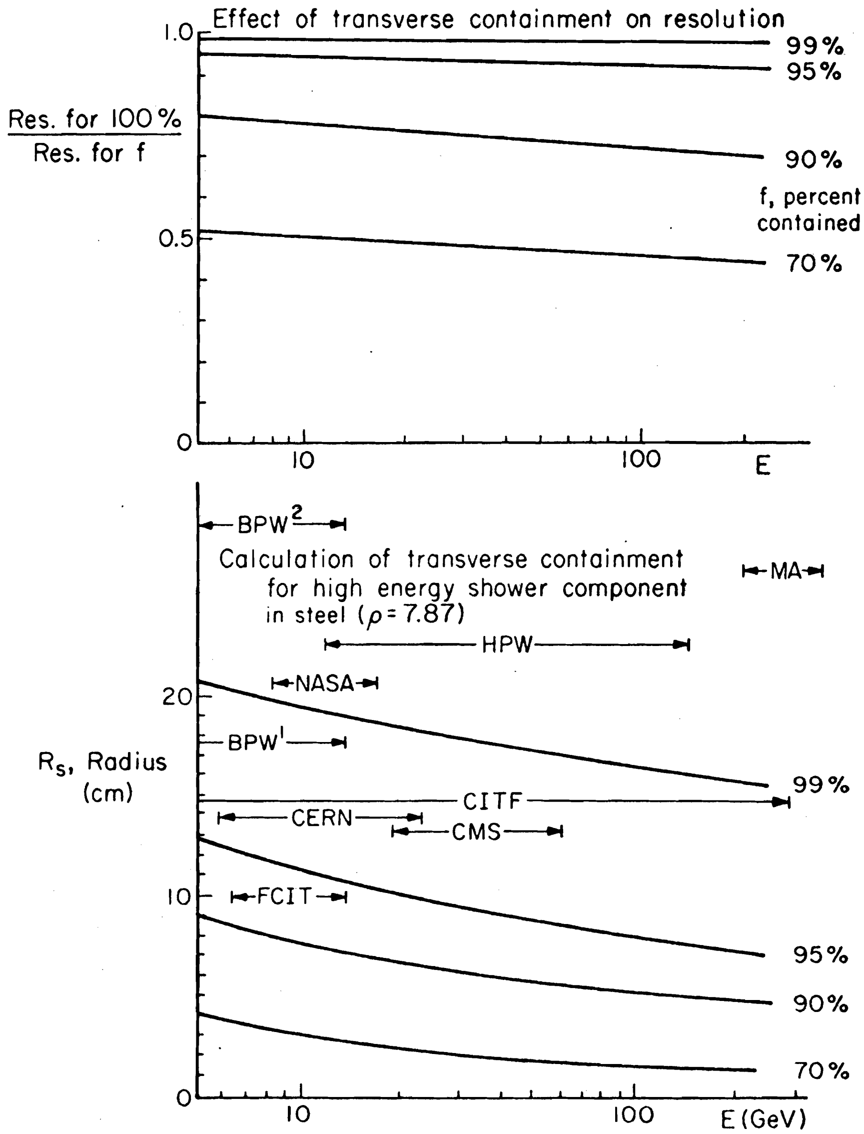

FIG. 15: Relative transverse containment for various calorimetry tests.

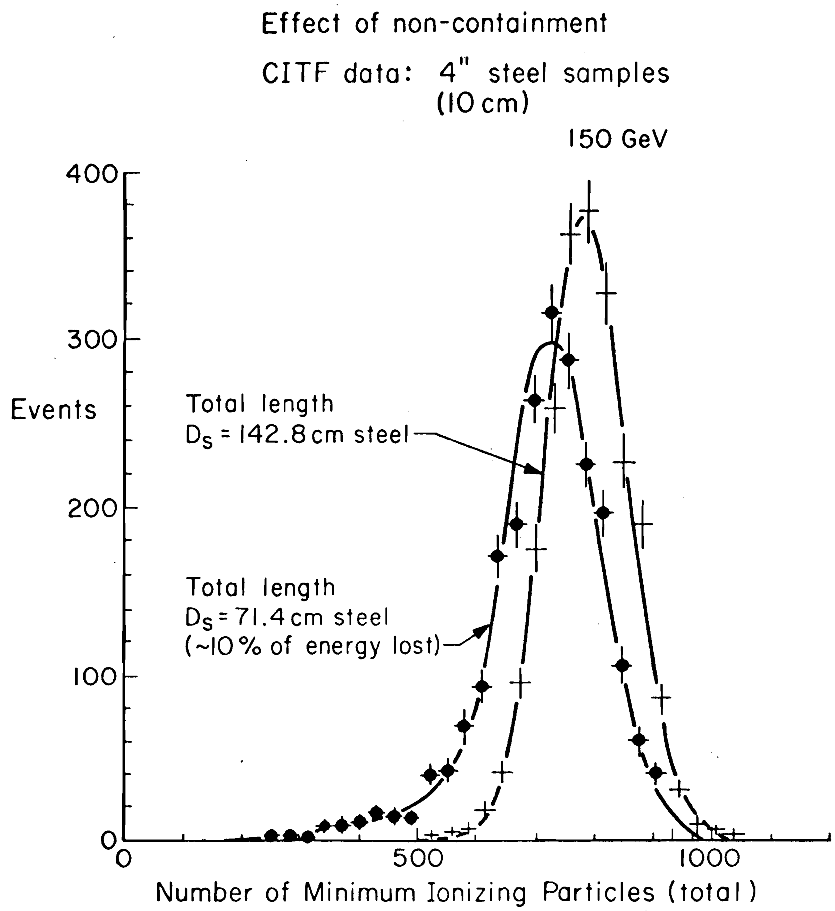

FIG. 16: Illustration of the development of low energy tails with poor containment.

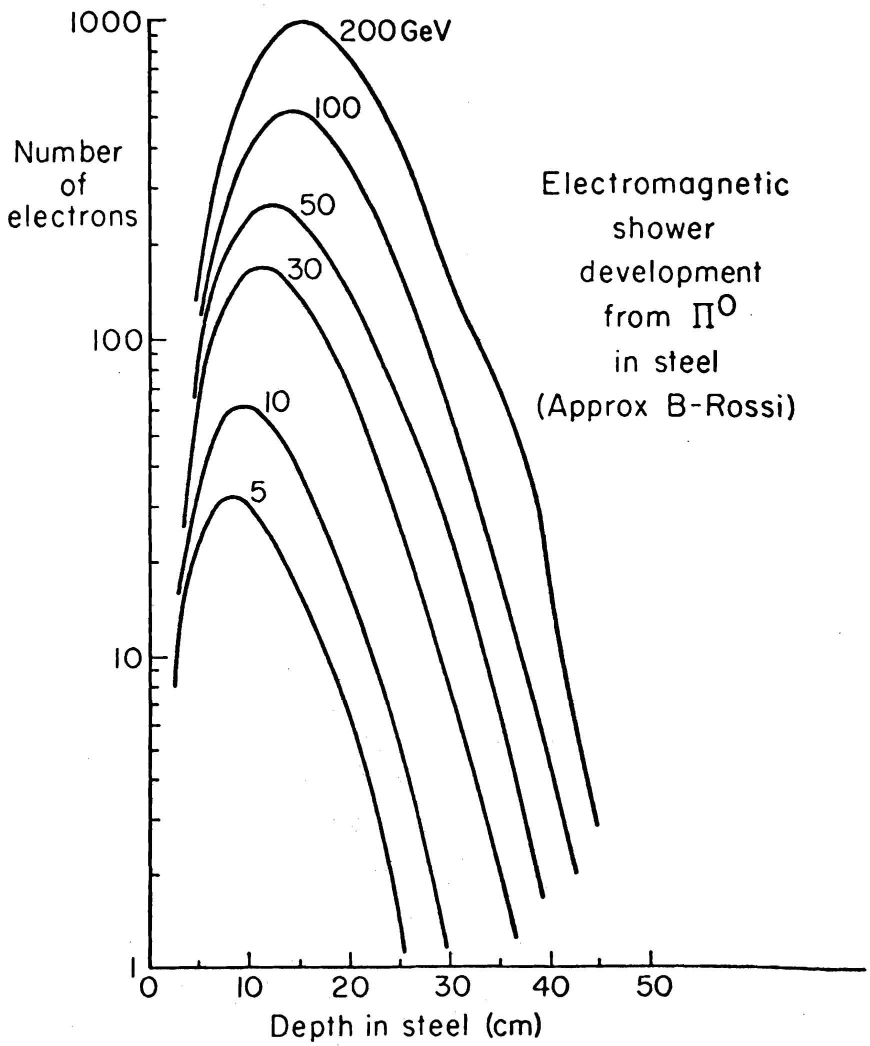

FIG. 17: Average electromagnetic shower development in steel.

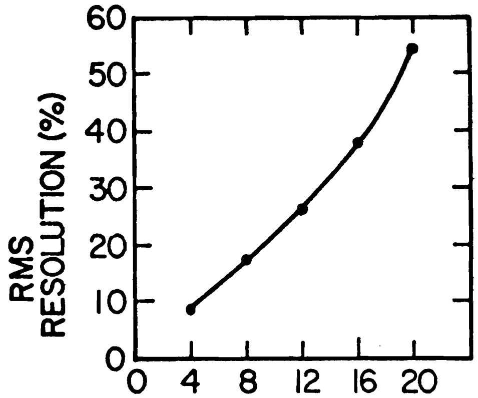

FIG. 18a: Effect on resolution of steel sampling distance, s; at 200 GeV.

RESOLUTION VS. SPACING 200 GeV

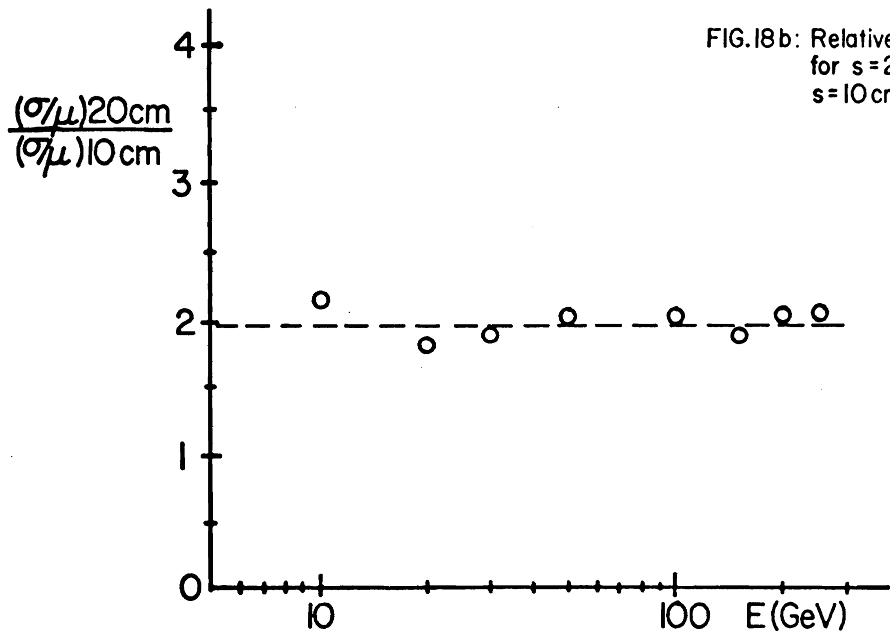

FIG. 18b: Relative resolution for s = 20cm to s = 10cm, vs. energy.

CITF DATA "THICK" SAMPLING

EFFECT ON RESOLUTION FOR 20cm STEEL SAMPLES RELATIVE TO 10cm SAMPLING

(CALT-68-494)

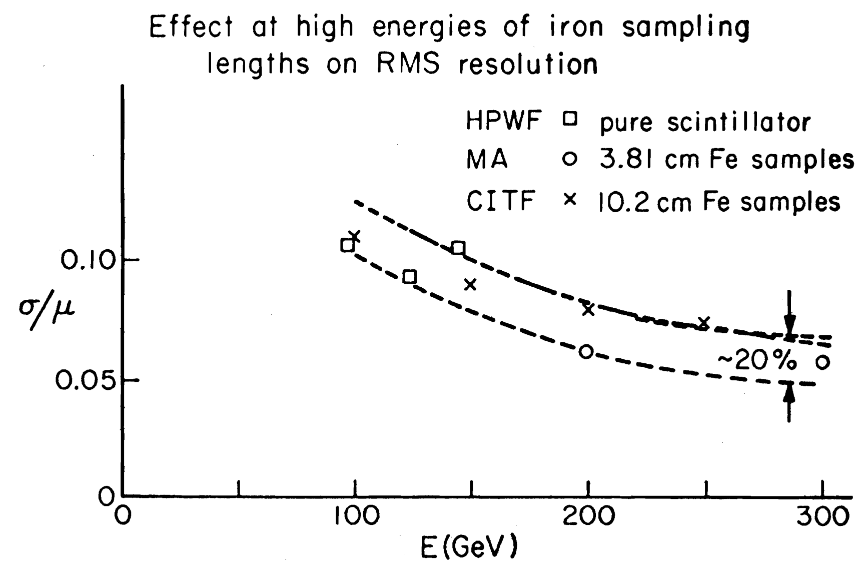
Effect at high energies of iron sampling lengths on RMS resolution
HPWF □ pure scintillator
MA ○ 3.81 cm Fe samples
CITF × 10.2 cm Fe samples
0.10
0.05
0
σ/μ
~20%
0
100
200
300
E(GeV)

FIG. 19

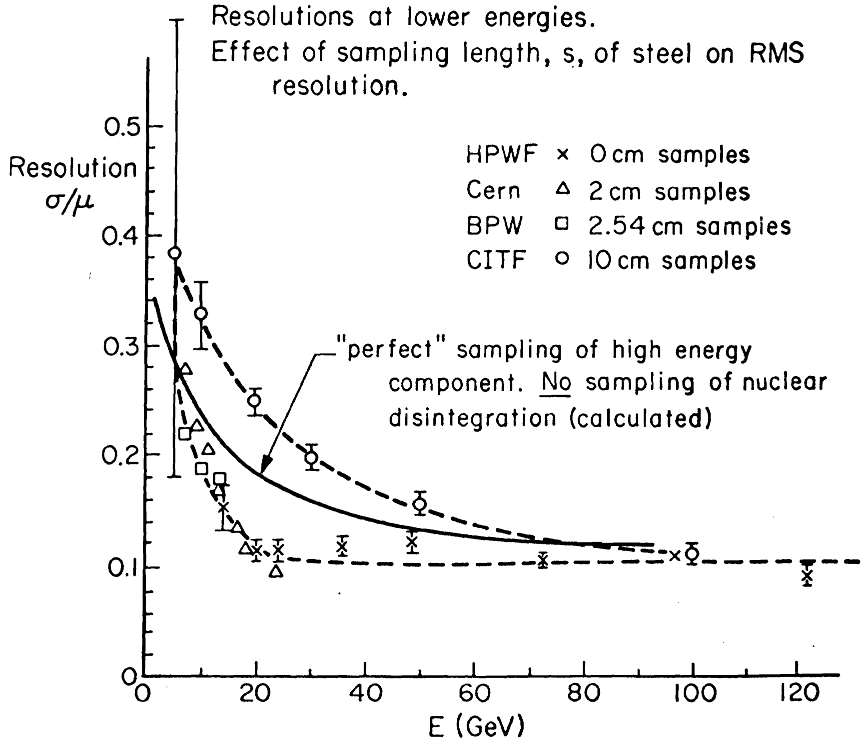
Resolutions at lower energies.
Effect of sampling length, s, of steel on RMS resolution.
HPWF × 0 cm samples
Cern △ 2 cm samples
BPW □ 2.54 cm samples
CITF ○ 10 cm samples
"perfect" sampling of high energy component. No sampling of nuclear disintegration (calculated)
Resolution σ/μ
0.5
0.4
0.3
0.2
0.1
0
0
20
40
60
80
100
120
E (GeV)

FIG. 20

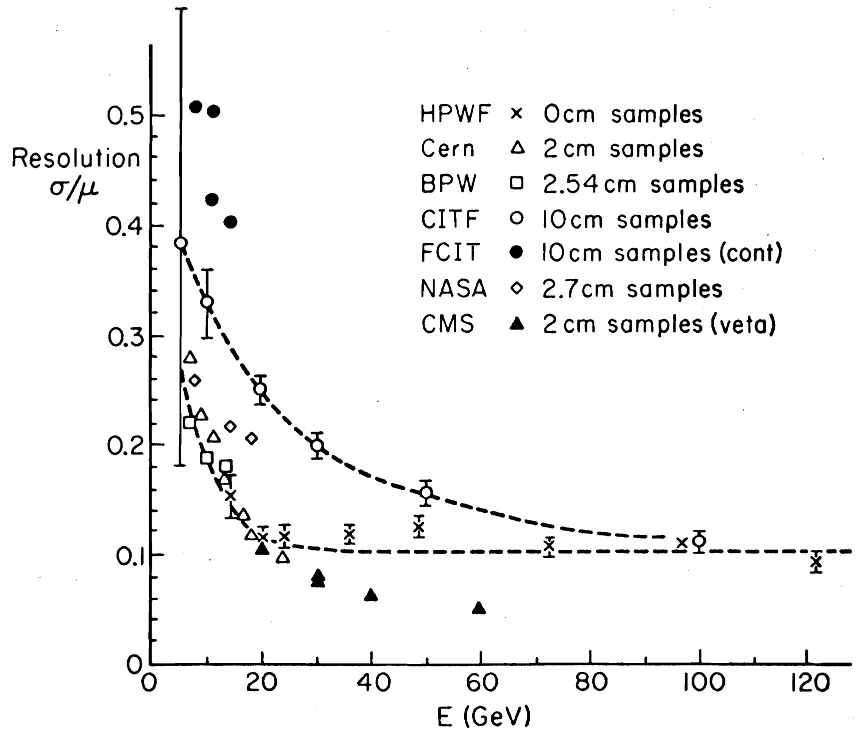
Resolution
σ/μ
0.5
0.4
0.3
0.2
0.1
0
0
20
40
60
80
100
120
E (GeV)
HPWF × 0cm samples
Cern △ 2cm samples
BPW □ 2.54cm samples
CITF ○ 10cm samples
FCIT ● 10cm samples (cont)
NASA ◇ 2.7cm samples
CMS ▲ 2cm samples (veta)

FIG. 21

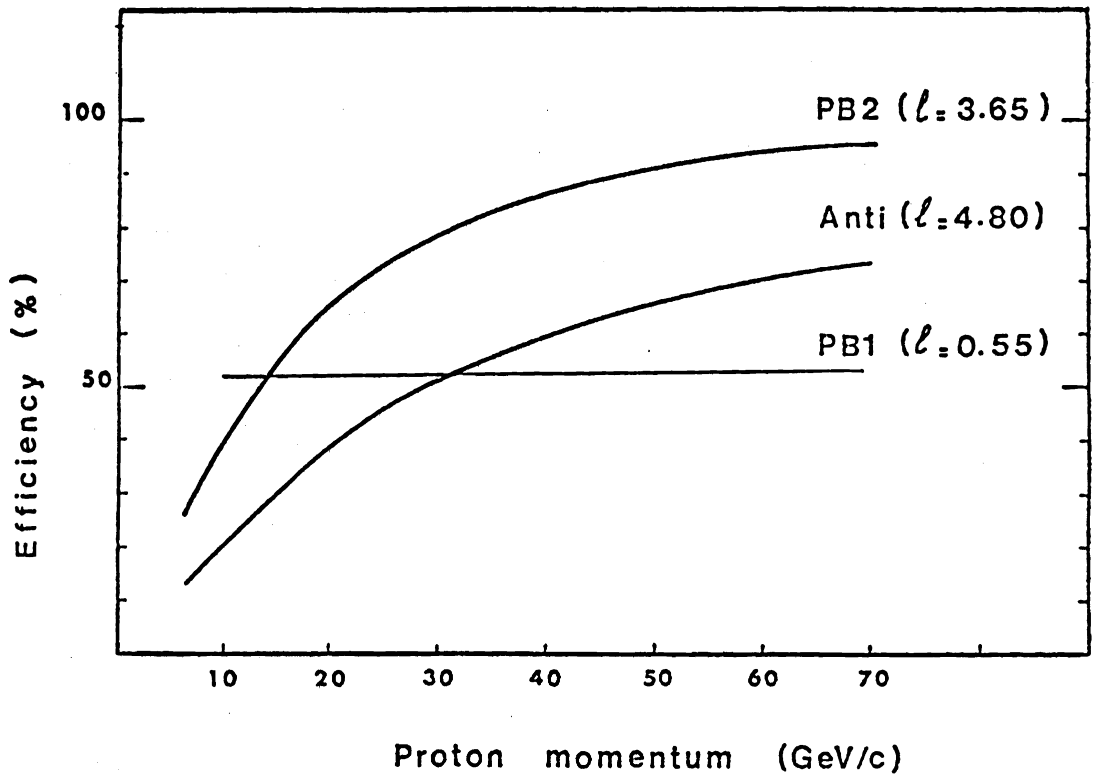
PB2 (ℓ=3.65)
Anti (ℓ=4.80)
PB1 (ℓ=0.55)
100
50
10
20
30
40
50
60
70
Efficiency (%)
Proton momentum (GeV/c)

FIG. 22

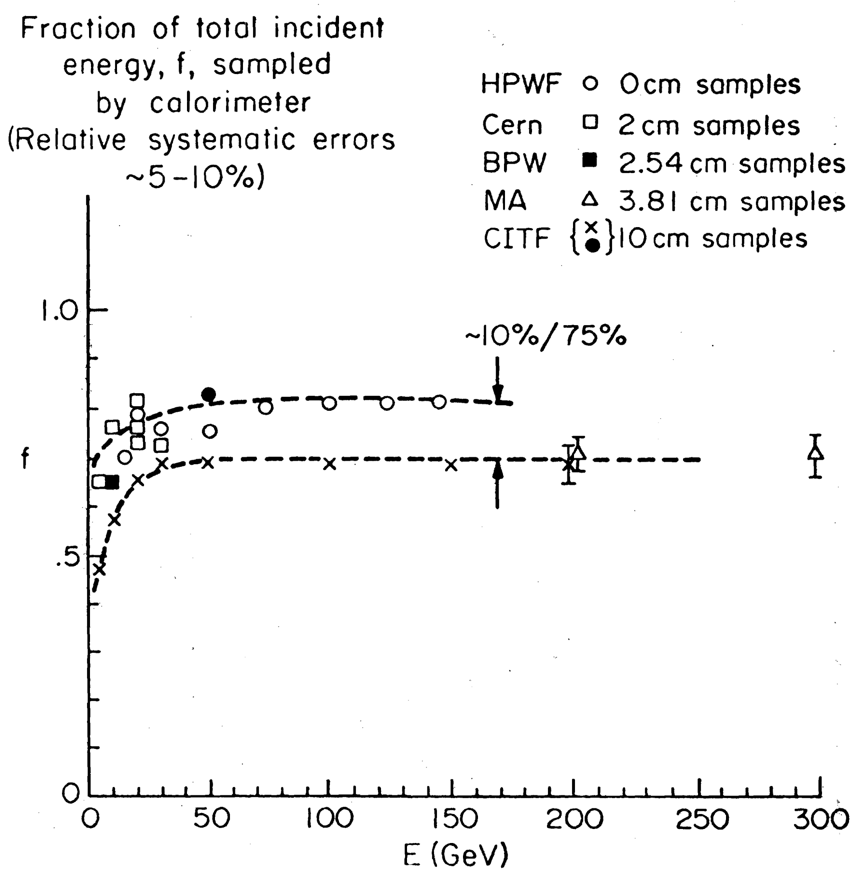
Fraction of total incident energy, f, sampled by calorimeter (Relative systematic errors ~5-10%)
HPWF ○ 0cm samples
Cern □ 2cm samples
BPW ■ 2.54cm samples
MA △ 3.81 cm samples
CITF {×●} 10cm samples
~10%/75%
1.0
f
.5
0
0
50
100
150
200
250
300
E (GeV)

FIG. 23

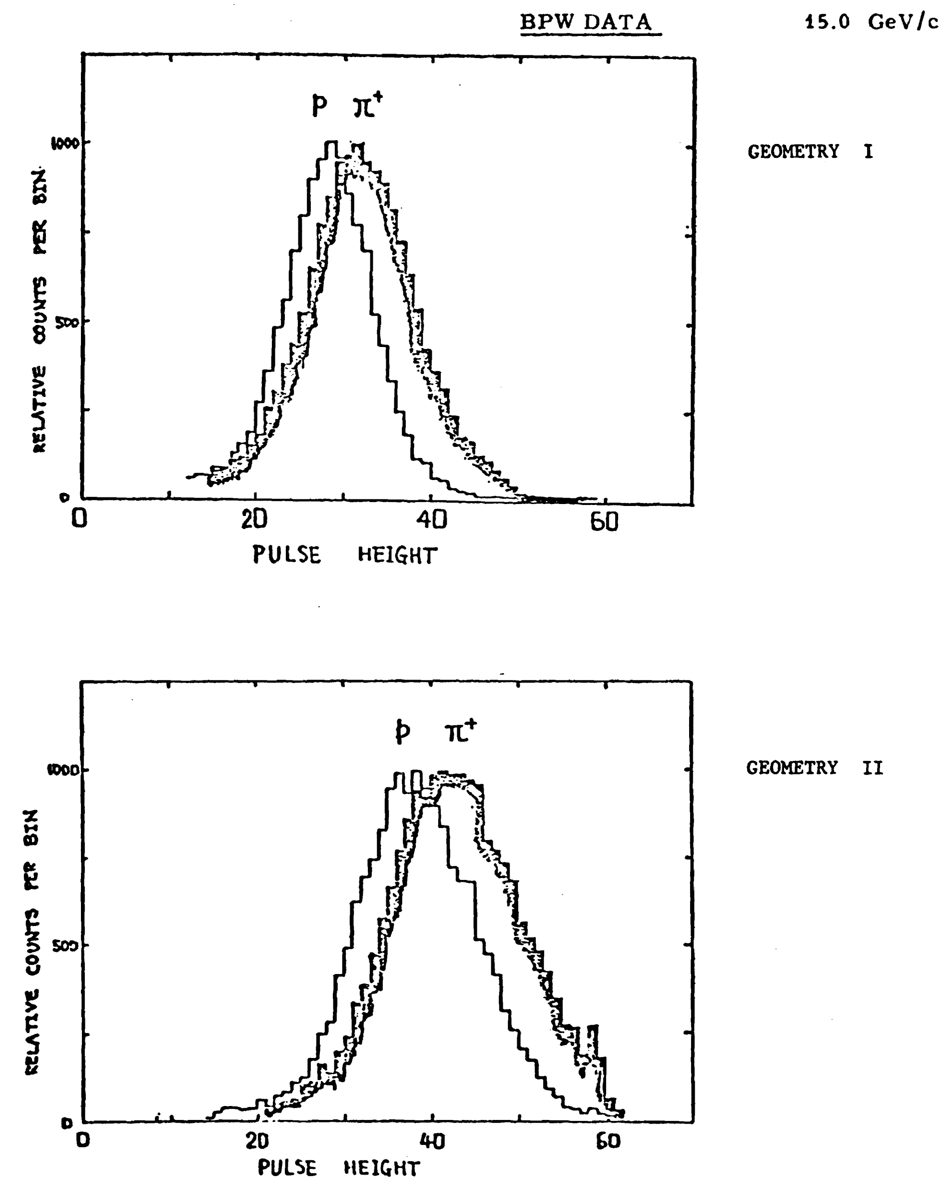
BPW DATA
15.0 GeV/c
p π+
RELATIVE COUNTS PER BIN
1000
500
0
0
20
40
60
PULSE HEIGHT
GEOMETRY I
p π+
RELATIVE COUNTS PER BIN
1000
500
0
0
20
40
60
PULSE HEIGHT
GEOMETRY II

FIG. 24

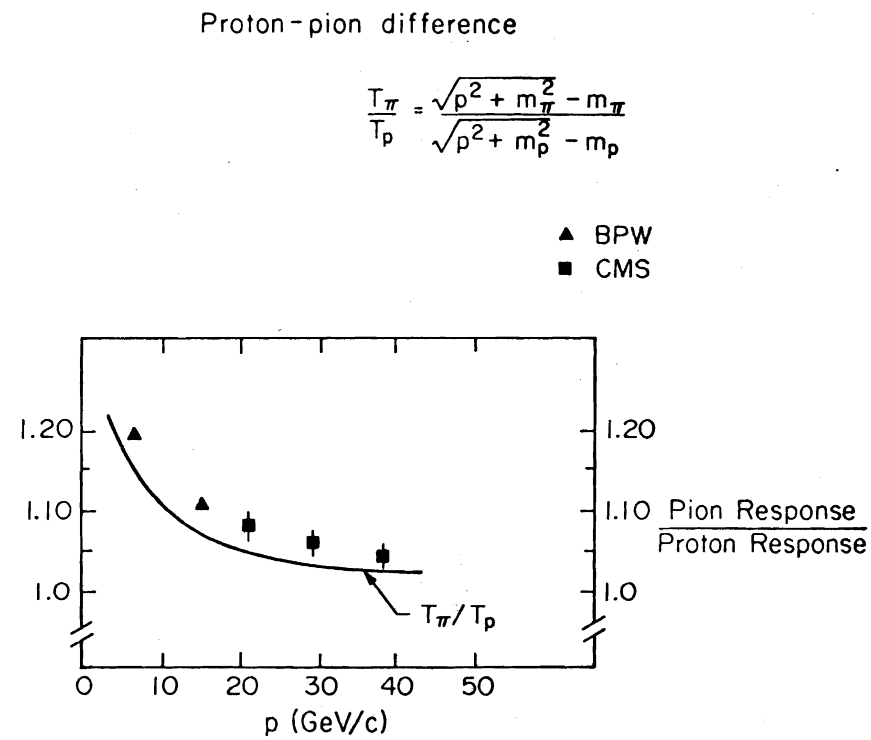
Proton-pion difference
$$\frac{T_\pi}{T_p} = \frac{\sqrt{p^2 + m_\pi^2} - m_\pi}{\sqrt{p^2 + m_p^2} - m_p}$$
▲ BPW
■ CMS
1.20
1.10
1.0
0
10
20
30
40
50
p (GeV/c)
T_π/T_p
Pion Response / Proton Response

FIG. 25